Localization of active pathways in peripheral nerves: A simulation study

José Zariffa, *Graduate Student Member, IEEE,* and Milos R. Popovic, *Senior Member, IEEE*

Abstract— A methodology is investigated for determining the location of active pathways in a peripheral nerve using measurements from a multi-contact cuff electrode. The problem is treated as an inverse problem of source localization and solved using the sLORETA algorithm, developed for the EEG/MEG source localization problem. Simulated measurements are generated corresponding to action potentials traveling along either one or three pathways in a rat sciatic nerve. The performance of the proposed methodology using these measurements is evaluated in terms of localization error, missed pathways, and spurious pathways. The source localization performance when assuming an idealized nerve anatomy is compared to that when the correct anatomy is known. The effect of a spatio-temporal constraint based on the nerve anatomy and electrophysiology is also investigated. The approach in its present form was not found to be sufficiently reliable for sub-fascicular localization in practice, due to mean localization errors in the 140μm-180μm range, high numbers of spurious pathways, and low resolution. Nonetheless, the constraints were shown to produce a marked reduction in the number of spurious pathways. Conditions under which the source localization approach may be useful for peripheral nerves are discussed.

Index Terms— Bioelectric source localization, cuff electrode, peripheral nerve interface, rat sciatic nerve, neural modeling.

I. INTRODUCTION

UNDERSTANDING the neural processes that underlie the functioning of the human body is an enormous task, which has led to countless studies of the central nervous system (CNS). Of course, although the actual information processing and control systems are located in the CNS, the control signals that flow in peripheral nerves are also a valuable source of information. Our ability to monitor the signals in specific neural pathways is, however, somewhat limited, particularly if the technology used must be appropriate for chronic implantation in humans. Methods or devices that improve our ability to localize bioelectric activity within a peripheral nerve would therefore be useful in several respects. Such technology would make it easier to characterize the control signals being exchanged between the CNS and a limb or organ, thereby allowing us to deepen our understanding of the neural systems governing processes such as reaching [1], bladder control [2], and many more. Furthermore, if the localization could be performed in real-time, the information exchange with a given limb could be monitored, interpreted, and used to control a neural prosthesis.

Current techniques for recording the electrical activity of peripheral nerves can be divided into two broad categories, each of which has shortcomings. Extraneural recordings, most commonly obtained using nerve cuff electrodes, can detect variations in the activity of the nerve as a whole, but techniques to determine the specific location of that activity within the nerve remain insufficient. In particular, the selectivity that can be achieved with cuff electrodes has been studied [3]–[6], but little work has been done on how to actually identify an arbitrary combination of active pathways using recordings from the surface of the nerve. Intraneural microelectrode arrays, on the other hand, can give us information about activity close to the tips of the microelectrodes, but arrays dense enough to achieve good coverage of the nerve are much more invasive than cuff electrodes, may inadvertently cause damage to the nerve when implanted or during movement, and may be too big for smaller nerves [7].

With this problem in mind, the simulation study presented here investigates a new strategy for localizing bioelectric activity in a peripheral nerve. Using potential recordings from multiple sites at the periphery of the nerve, obtained from a multi-contact cuff electrode, the problem can be formulated as a modified version of the distributed electroencephalogram/magnetoencephalogram (EEG/MEG) source localization problem [8]–[13]. Although the proposed scheme essentially falls into the category of extraneural recording methods, it is differentiated from previous studies both in the details of the instrumentation (i.e. the number of contacts placed in the cuff electrode) and of the data processing algorithm (nerve cuff recordings are usually examined with traditional signal processing algorithms [14]–[17], whereas here we use techniques from the field of inverse problems). Some attempts have been made to separate the activity of different fascicles in a nerve based on extraneural recordings, using either blind source separation [18] or linear regression [19], [20]; the method proposed here in effect generalizes these ideas and aims to obtain a more flexible framework, suitable for differentiating activity not only between fascicles but also within a single fascicle (albeit with limited resolution). A similar source localization approach has been suggested for the purposes of electrode targeting in the spinal cord [21].

The authors are with the Institute of Biomaterials and Biomedical Engineering, University of Toronto, the Edward S. Rogers Sr. Department of Electrical and Computer Engineering, University of Toronto, and the Toronto Rehabilitation Institute, Toronto, Canada. Email: jose.zariffa@utoronto.ca.

II. METHODS

A. Approach to solving the source localization problem

In order to obtain an estimate of the source distribution from the cuff electrode measurements, there are two problems that need to be addressed: the forward and the inverse problem. The goal of the forward problem is to compute the measured potentials that would result at each contact from a source at a given location. This information can be represented in matrix form, and is known as the leadfield matrix. The leadfield is needed to solve the inverse problem, whose goal is to estimate the source distribution from the measurements.

Due to the ill-posed and underdetermined nature of the inverse problem of bioelectric source localization, in order to arrive at a unique solution it is necessary to impose constraints on the solution [22]. These constraints should be determined by the anatomical and physiological features of the problem at hand. In our simulations, we will investigate the performance of the source localization approach when varying levels of information about the nerve are incorporated into the problem. An overview of the process is given below, and details about each aspect of the simulations are presented in the following sections.

- First, create two numerical models of the nerve: a) one with an idealized geometry and b) the other with a more realistic geometry. A leadfield is generated from each model, and the more realistic model is used to generate simulated measurements, which will be used in all simulations.
- Second, develop a spatio-temporal constraint based on the electrophysiological behaviour of myelinated axons.
- Third, evaluate the localization performance in four cases, which are: (1) using the idealized leadfield and no spatio-temporal constraint (case IL), (2) using the idealized leadfield and the spatio-temporal constraint (IL-C), (3) using the correct leadfield (i.e. the one obtained from the more realistic geometry and used to generate the measurements) and no spatio-temporal constraint (CL), and (4) using the correct leadfield and the spatio-temporal constraint (CL-C). The first of theses cases incorporates the least information about the problem into the inverse problem solution, whereas the last case incorporates the most information.

1) The forward problem: The forward problem is well-defined and can be solved analytically for simple geometries and conductivity distributions. Unfortunately, the anisotropic conductivity of nerves and the potentially irregular shape of the fascicles mean that we must resort to numerical techniques. Specifically, the forward problem is solved using finite-element modeling (FEM). In EEG/MEG source localization, the method of choice is often the boundary-element method (e.g. [23]–[25]), but FEM is better suited to anisotropic conductivities [26], [27] and for that reason is used here.

The first FEM model was built based on the idealized geometry of a unifascicular section of the rat sciatic nerve. This extended unifascicular geometry is a simplification compared to the real anatomy, which would branch progressively into several fascicles. The main components of the model were a

TABLE I
PARAMETERS FOR THE IDEALIZED FINITE ELEMENT MODEL OF THE RAT SCIATIC NERVE

Parameter	Values	References
Nerve length	5 cm	
Endoneurium radius	360 μm	[29]
Perineurium width	25 μm	[4]
Epineurium width	35 μm	[30], [31]
Encapsulation tissue layer width	40 μm	[4]
Saline layer width	40 μm	[4], [31]
Cuff length	2.3 cm	[28]
Cuff width	30 μm	[28]
Cuff radius	500 μm	[28]
Cuff starting height	1.35 cm	
Saline bath length	5 cm	
Saline bath radius	0.48 cm	[4], [6]
Endoneurium conductivity (radial)	8.26×10^{-2} S/m	[6], [30], [32]
Endoneurium conductivity (longitudinal)	0.571 S/m	[30], [32], [6], [33]
Perineurium conductivity (all directions)	2.1×10^{-3} S/m	[6], [30], [33]
Epineurium conductivity (all directions)	8.26×10^{-2} S/m	[6], [33]
Encapsulation tissue conductivity (all directions)	6.59×10^{-2} S/m	[31]
Saline conductivity (all directions)	2 S/m	[30], [31], [6], [33]
Cuff conductivity (all directions)	1×10^{-7} S/m	[6]

cylindrical nerve surrounded by a cuff electrode and placed in a saline bath. The nerve was modeled as three concentric cylinders representing the endoneurium, perineurium and epineurium layers. The nerve and the cuff were separated by an encapsulation tissue layer and a saline layer (left panel of Figure 1). The dimensions and conductivities of the various part of the nerve model are given in Table I and based on related models and anatomical studies described in the literature. 56 electrode contacts were placed on the inside of the nerve cuff, organized in 7 rings of 8 electrodes each. The dimensions of the cuff electrode and the layout of its contacts are based on an existing "matrix" cuff electrode [28]. The ratio of the bath and nerve diameters is large enough to avoid boundary effects [6], and the nerve segment is long enough that dipoles placed at its ends have a negligible impact on the measurements. The number of mesh elements in the model's endoneurium was 56,400.

The second FEM model was based on a trace of a cross-section of a rat sciatic nerve, at the level where the nerve begins to divide into its tibial and peroneal branches. The image that formed the basis of the trace was obtained from the literature (Figure 1C in [29]). The dimensions of the cuff and the bath were the same as in the previous model, as were the conductivities. In order to fit the nerve into the cuff, it was scaled to 90% of its original size. This is a considerably simpler process than morphing the mesh to conform to the shape of the cuff, and was deemed acceptable for the purposes of this study. It is important to clarify that this geometry is still simplified, in that it is uniform in the longitudinal direction, and as such does not represent the progressive branching of the nerve. The cross-section that was selected as the basis for the trace was chosen because it corresponds approximately to where the half-point of the cuff would be located on the
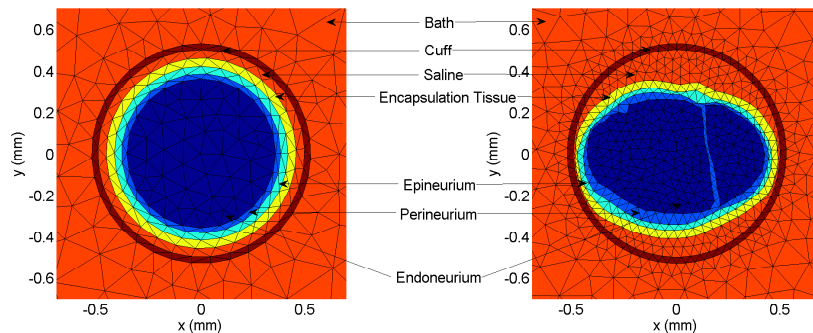
Fig. 1. Cross-sections of the idealized (left) and more realistic (right) FEM model geometries used to construct the leadfields.

sciatic nerve, assuming the cuff was implanted just proximal to the division of the nerve into its main branches. It has been shown that the shape of the nerve will conform to that of the cuff during chronic implantation [34]. Therefore, the geometry used here corresponds to a situation in which the cuff has only been implanted for a short time, which is interesting for the purposes of this study, because the difference between the "realistic" geometry and the idealized one will be greatest at that time. The cross-sections of both FEM models are shown in Figure 1. The number of mesh elements in the second model's endoneurium was 218,400 (the more complex geometry required a finer mesh).

The finite element analysis was conducted using the SCIRun computing environment [35], and the rest of the leadfield computations were performed using the Matlab software. The procedure for obtaining the leadfield from the finite element model is described by Weinstein *et al.* [26].

2) Simulated measurements: To generate simulated measurements, a myelinated mammalian nerve fiber action potential was first simulated using the model described by Sweeney *et al.* [36]. In order to remain consistent with the EEG/MEG source localization literature, equivalent current dipoles were used to model the electrical activity of the nerve fibers. The magnitude waveform of the current dipole was therefore obtained from the first derivative of the transmembrane potential during the action potential [37]. The waveform was then propagated from one node of Ranvier to the next at a speed of approximately 50m/s [36]. The nodes of Ranvier were placed 1mm apart, which is consistent with a 10μm-diameter fiber. The length of the simulation was 2ms.

Once the location and time course of the current sources had been determined, the simulated measurements at the electrode contacts were obtained using the second FEM model described in the previous section. The reference for the measurements was the average of the two reference contacts present in the "matrix" cuff design (see [28]). Noise was then added to each set of measurements, with the noise standard deviation set to 0%, 10%, 20%, 30%, and 40% of the signal standard deviation. The signal standard deviation for the purposes of generating the noise was estimated by computing the standard deviations of the measurements at each of the 8 contacts in the middle

ring of the cuff, then averaging those values. The resulting noise standard deviation was used to generate Gaussian white noise time series for each of the 56 contacts. This noise represents the remaining contamination after appropriate filtering and noise reduction measures have been used.

Measurements corresponding to two situations were simulated: a single active fiber, and three active fibers. Each of the two cases was repeated 100 times, with the positions of the active fibers within the endoneurium generated randomly every time. For the case of three active fibers, the waveforms for all three fibers were identical but a random time shift was applied. The maximum allowable time shift was a quarter of the length of the simulation. Given the distance between the nodes of Ranvier and the length of the nerve model, each fiber was composed of 50 dipoles, each with its own time course. The source localization task described in the following sections was therefore dealing with regions featuring either 50 or 150 dipoles with varying magnitudes.

3) The inverse problem: There are two broad categories of EEG/MEG source localization methods: equivalent dipole methods and distributed linear methods. Equivalent dipole methods assume that the potential measurements can be explained using a small number of equivalent dipoles, whose number is set *a priori* or estimated using the data and whose location, orientation, and magnitude must be determined using search algorithms to fit the measurements [38], [39]. In the peripheral nerve problem, the combination of multiple active fibers and the distribution of activity along the length of the fibers make the assumption of a small number of dipoles very hard to justify. The distributed linear methods, on the other hand, formulate the problem as the estimation of the magnitudes of a large number of dipoles whose locations and orientations are fixed. Electric fields add linearly, so the relationship between the measurements and the dipole magnitudes can be expressed as the linear system in Equation 1.

$$\mathbf{d}(n) = \mathbf{L}\mathbf{j}(n) + \epsilon(n) \qquad (1)$$

Here, $\mathbf{d}(n)$ is the Mx1 vector of measurements at instant n, $\mathbf{j}(n)$ is the 3Nx1 vector of current dipole magnitudes at instant

n, and $\epsilon(n)$ is additive noise (assumed Gaussian). The Mx3N matrix $\mathbf{L}$ is the leadfield matrix, which relates the potential measurement at each electrode contact to the existence of a unit source at each possible location. It is constructed as described in Section II-A.1. There are three leadfield columns for each of N mesh elements, corresponding to the three orthogonal dipole orientations. Note that the system at each time instant can be considered as independent of the other time instants because quasistatic conditions hold [40].

The difficulty of recovering $\mathbf{j}(n)$ from $\mathbf{d}(n)$ and $\mathbf{L}$ comes from the fact that the problem is underdetermined and ill-posed. In order to obtain a stable solution, additional constraints must be added to the problem. A number of reviews are available that give an overview of the most commonly used types of constraints [22], [41]. Here, the method chosen is the standardized low resolution brain electromagnetic tomography (sLORETA) method [10]. In the absence of additional information about the solution, sLORETA usually outperforms other instantaneous distributed linear methods, but does this at the cost of decreased spatial resolution. In other words, it produces images that are blurred but have well-localized peaks; this smoothness is imposed on the solution as a constraint to deal with the ill-posed nature of the problem. The algorithm has been shown to localize single sources with zero error in the noiseless case [10]. sLORETA consists of two steps: first, a regularized minimum-norm least-squares solution of Equation 1 is obtained; second, that solution is normalized using the diagonal of the resolution matrix, which provides information about the bias of the solution for each entry in $\mathbf{j}(n)$. The regularization parameter is chosen here by means of the cross-validation error function, as suggested by Pascual-Marqui [10], [42].

Our choice of algorithm is based on three criteria. First, it should not make the assumption that there are only a small number of active sources, as was already discussed above. Second, it should be reasonably fast, in view of possible application in a neuroprosthetic system. Lastly, it should not assume that the source distribution generating the measurements is stationary over a certain time interval, because outside of a controlled experiment there would be no way to ensure that the set of active pathways is not changing over the observation period. sLORETA satisfies all three of these requirements.

In order to reduce the number of variables that need to be solved for in the inverse problem, we can further restrict the location and orientation of the dipoles. Active fibers can only be located in the endoneurium, so the perineurium and epineurium regions are removed from the solution space. The current dipoles that are used to model the extracellular field of an action potential are oriented axially along the fiber [40], so that dipoles in the other two orthogonal directions can be eliminated from consideration, thereby reducing the number of variables by two thirds.

4) Spatio-temporal constraint: Keeping in mind that the basic approach to solving underdetermined inverse problems is to constrain the solution based on our knowledge of the problem, we investigate a spatio-temporal constraint based on the electrophysiology of nerve fibers. Assuming that we are applying what follows to myelinated fibres, a spatio-

temporal constraint can be implemented based on the formula in Equation 2.

$$V(x,t) = V(x - ds, t - ds/v) \qquad (2)$$

V(x,t) is the transmembrane voltage at position x along the fibre and at time t, ds is the spatial distance separating two consecutive nodes of Ranvier, and v is the conduction velocity. ds and v can be estimated from the diameter and type of the fibre. The formula is simply saying that the activity at a node is ideally identical to the activity at the previous node ds/v seconds in the past.

Putting this equation to use assumes that the type (myelinated vs. unmyelinated) and diameter of the fibres at a given location in the nerve are known. Alternatively, even if no information about the location of different fibre types is available, the constraint can be applied if a single type of fiber is active at a given time, by assuming that the whole nerve is composed of fibers of that type. In that situation, before performing the localization, one can identify the nerve conduction velocity (and thus fiber type) from the multi-contact cuff electrode using a method such as the one proposed by Rieger et al. [43].

In order to incorporate this information as a constraint, temporal coupling must be introduced into the problem. Ideally, the whole spatio-temporal system could be expressed and solved as a single linear system, by concatenating the measurement and source vectors for all time instants [44], [45]. This is shown in Equation 3, which is very similar to Equation 1, with the exception that the vectors $\mathbf{d_c}$, $\mathbf{j_c}$, and $\epsilon_\mathbf{c}$ include the complete information about the system at all time instants in the observation time window (i.e. $\mathbf{d_c} = [\mathbf{d}(1)^\mathbf{T}\mathbf{d}(2)^\mathbf{T}...\mathbf{d}(n)^\mathbf{T}]^\mathbf{T}$, with equivalent definitions for $\mathbf{j_c}$ and $\epsilon_\mathbf{c}$, and n being the total number of time samples). $\mathbf{L_c}$ is a block diagonal matrix, where each block is equal to $\mathbf{L}$.

$$\mathbf{d_c} = \mathbf{L_c}\mathbf{j_c} + \epsilon_\mathbf{c} \qquad (3)$$

The problem with this approach is that the number of variables is multiplied by the number of time instants, making the system intractable for any realistic application. Therefore, for computational reasons, we restrict ourselves to coupling two time instants at a time. Specifically, in accordance with Equation 2, we solve the systems corresponding to the pairs of time instants (t(1), t(1)+ds/v), (t(2), t(2)+ds/v), etc. ds/v is rounded to the nearest integer. To couple the solutions of the two time instants together in the desired manner, a coupled leadfield and a non-diagonal weight matrix are constructed as shown in Equation 4. In general, the weight matrix in a distributed linear method for this type of problem is applied to the norm of the solution in the minimum-norm least-squares problem and is used to apply *a priori* constraints to the solution. The incorporation of a weight matrix into the sLORETA algorithm is described in the original paper by Pascual-Marqui [10].

$$L_c = \left[\begin{array}{cc} L & 0 \\ 0 & L \end{array} \right] \quad H_c = \left[\begin{array}{cc} I & -A \\ 0 & I \end{array} \right] \qquad (4)$$

I is the identity matrix corresponding to the number of variables in a single time instant, and A contains the spatial element of the constraint. If elements i and j of the solution vector correspond to locations along the same pathway and separated by a distance ds, then $A_{i,j}$ is set to 1. In this way, each row of A corresponding to a location in a constrained pathway contains a single entry of value 1. H_c therefore constrains those values in the solution at time t+ds/v to have as close a value as possible to the element situated ds lower in the solution at time t by penalizing differences in these values, as desired.

In the case of our simulations, the constraint assumed that the whole nerve was composed of myelinated fibres of diameter 10μm with nodes of Ranvier spaced 1mm apart and a conduction velocity of 50m/s. These values are the same as the ones used to generate the simulated measurements.

B. Evaluation of the results

The characteristic of the solution that is of most interest to us is the position of the active pathways. For that reason, we are primarily interested in the position of the sources in a cross-section of the nerve, rather than in their longitudinal position. The three-dimensional solution can therefore be projected onto a two-dimensional cross-section for the purposes of computing an error metric. This is done by summing the absolute values of the activity of all the mesh elements with the same cross-sectional position. The value associated with each location in the resulting two-dimensional projection is therefore a representation of how much activity was spread along the length of the nerve at that position. This process implies that a nerve fibre has a straight path with very little radial deviation along the length of the nerve segment; because there may in fact be small deviations *in vivo*, we stress that the actual source localization in no way depends on this assumption. It is simply used to obtain useful metrics to evaluate the performance of the method in the context of the simulations, and is justified here because the simulated nerve fibres were in fact straight.

To further simplify the evaluation of the localization process and obtain concise metrics, we sum the estimates from all the time instants of a given trial before performing the two-dimensional projection. The three-dimensional activity over the time interval is therefore summarized as a single two-dimensional source distribution. It is important to clarify that summing the estimates of all the time instants does not presuppose stationarity of the underlying sources; it simply provides an indication of what sources were active at some point in the time interval.

Lastly, the estimated source locations are obtained by finding the local maxima in the final two-dimensional projection. These local maxima are used to estimate the localization error, as well as the number of missed and spurious pathways. The metrics are computed as follows:

1) The mesh is interpolated onto a regular grid. The local maxima are detected on this grid by comparing the activity at each location with the activity at all locations within 50μm. The peak coordinates are obtained, and the results mapped back onto the FEM mesh cross-section.

2) Each peak in the estimate is associated with the true pathway closest to it. A localization error is obtained for each of the true pathways by computing the peak-to-peak distance between that pathway and the closest of the estimated peaks assigned to it. The other peaks associated with that true pathway, if any, are counted as spurious peaks.

3) True pathways that do not have any peaks associated with them in Step 2 are counted as missed pathways.

III. RESULTS

A. One-pathway case

The mean values over 100 trials of the localization error, number of spurious pathways, and number of missed pathways when a single true pathway is present are shown in Figure 2. When the idealized leadfield was used with no constraints, the localization error was relatively independent of the noise level, with non-monotonic variations between a minimum of 0.137mm and a maximum of 0.166mm. When the spatio-temporal constraint was added, similar non-monotonic variations were observed between a minimum of 0.134mm and a maximum of 0.182mm. When the correct leadfield was used, a clear relationship with the noise was observed: the error increase monotonically from 0.078mm to 0.166mm without the spatio-temporal constraint, and from 0.081mm to 0.175mm with the constraint. The statistical significance of this finding was confirmed by the fact that, when testing the relationship between error and noise against a null hypothesis of no correlation, *p* was less than 0.05 only in the cases where the correct leadfield was used. The difference in results between the simulations with the idealized leadfield and those with the correct one is due to the geometry error. In other words, even when the amount of measurement noise is low, the localization algorithm must still deal with a large amount of error if the leadfield is based on an inaccurate model of the region. The relatively constant error in the idealized leadfield cases additionally seems to suggest that there is a plateau in the amount of localization error as the noise increases, at least for the range of values examined.

Spurious pathways were seen to constitute the biggest obstacle to the applicability of the source localization approach. The number of spurious pathways increased monotonically with the noise in all cases (this relationship was statistically significant in all cases except IL, possibly because the number of spurious pathways seems to reach a plateau early in that situation). When the idealized leadfield was used, the metric varied from 1.05 to 3.24. When the spatio-temporal constraint was added, the range of values was from 1.14 to 2.51. When the correct leadfield was used without the constraint, the range was 0.02 to 2.62, and with the constraint it was 0.06 to 1.74. As clearly visible in Figure 2, this data reveals that the amount of information incorporated into the source localization problem has a direct impact on the number of spurious pathways: the spatio-temporal constraint led to a marked decrease regardless of the leadfield used, and the combination of the correct mesh with the constraint noticeably outperformed all of the other cases. One-way ANOVA followed by a multiple comparison
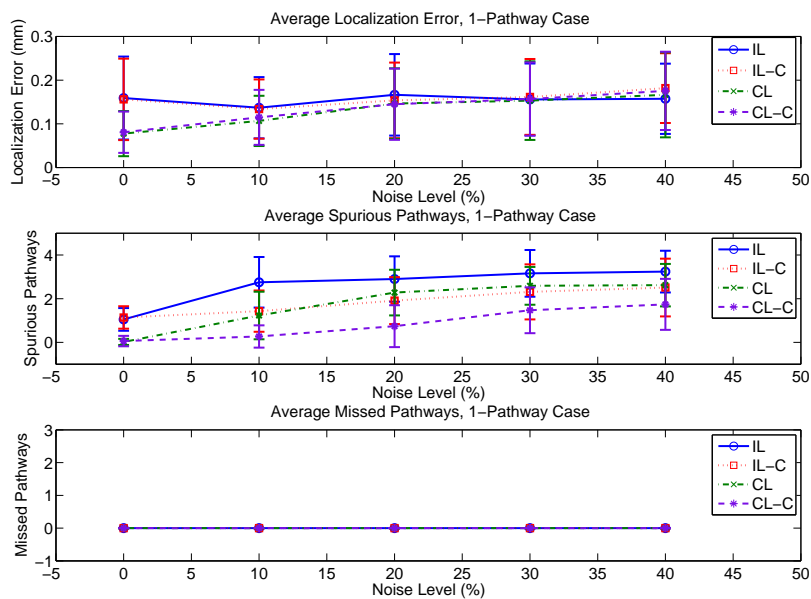
Fig. 2. Localization errors, spurious pathways, and missed pathways for the one-pathway case (n = 100). IL: idealized leadfield; IL-C: idealized leadfield with spatio-temporal constraint; CL: correct leadfield; CL-C: correct leadfield with spatio-temporal constraint.

test between the four cases, performed at every noise level, showed statistically significant ($p < 0.05$) differences between all pairs except the pair (IL-C, CL). This confirmed the differences qualitatively visible in Figure 2. The exception was the 0% noise case, in which the choice of leadfield led to significant differences but the spatio-temporal constraint did not. Overall, the presence of the spatio-temporal constraint led to minor increases in localization error at high noise levels, but marked reductions in the number of spurious pathways, which seems to be a worthwhile trade-off. The error increase was not statistically significant ($p > 0.05$), and may be due to the larger number of variables in the coupled problem. No missed pathways were observed, which is not surprising given that a single pathway was present in the region.

Figure 3 (panels a), c) and e)) shows an example of a localization trial. The smoothing effect of sLORETA is clearly visible, as is the presence of spurious pathways. Note that the trials shown in this figure (for both the one- and three-pathways cases) are selected to help the reader visualize the concepts being discussed; they are not necessarily the most representative of the method's performance. For that information, the reader should rely rather on the metrics discussed in the text and shown in Figures 2 and 4.

B. Three-pathways case

Panels b), d), and f) of Figure 3 show an example trial for the three-pathways case. The mean values over 100 trials of the localization error, number of missed pathways, and number of spurious pathways when three true pathways are present are shown in Figure 4. The localization error when the idealized leadfield was used with no constraints was again relatively independent of the noise level ($p > 0.05$ under a null hypothesis of no correlation), varying non-monotonically between

0.152mm to 0.181mm. With the spatio-temporal constraint, the range was 0.155mm to 0.179mm. The errors when the correct leadfield was used were once again an increasing function of the noise ($p < 0.05$), ranging from 0.083mm to 0.182mm without the constraint, and from 0.087mm to 0.180mm with the constraint. These results are very similar to those seen in the one-pathway case.

The general trends for spurious pathways were also similar to those in the one-pathway case, including the effects of the constraints. Although the increase with noise was not strictly monotonic in all cases, that was nonetheless the trend ($p < 0.05$ in all four cases). The number of spurious pathways when the idealized leadfield was used varied from 0.47 to 1.72 without the constraint, and from 0.64 to 1.15 with the constraint. When the correct leadfield was used, the range was from 0.02 to 1.24 without the constraint, and from 0.02 to 0.88 with the constraint.

When multiple true pathways were present, the number of missed pathways increased dramatically. The general trend was an overall decrease as the amount of noise increased, although this proved statistically significant only in the cases with the correct leadfield. When the idealized leadfield was used, the number of missed pathways ranged from 0.84 to 0.31 without the constraint, and from 0.84 to 0.58 with the constraint. When the correct leadfield was used, the range was from 1.44 to 0.38 without the constraint, and from 1.57 to 0.62 with the constraint.

IV. DISCUSSION

The localization of active pathways in a peripheral nerve was approached as an inverse problem of bioelectric source localization, using simulated measurements from a 56-contact nerve cuff electrode. This is an ill-posed inverse problem,
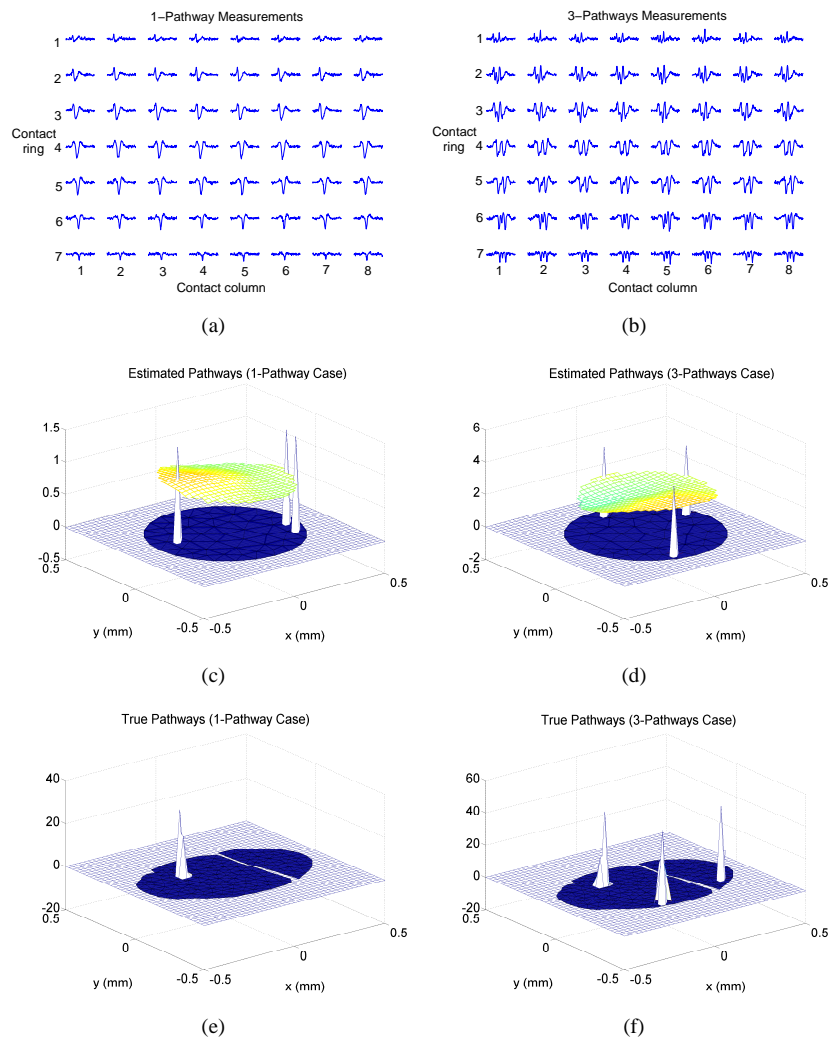
Fig. 3. Figure a) shows the normalized simulated measurements obtained at all 56 contacts (7 rings of 8 contacts) for one of the one-pathway trials. The noise level is 20%. Figure c) shows the estimated pathways obtained by applying the source localization procedures to the measurements in a), using the idealized leadfield combined with the spatio-temporal constraint. Figure e) shows the true location of the pathway for this trial. Figures b), d), and f) show equivalent data for one of the three-pathways trials. The sharp peaks seen in the estimates are not part of the source localization solution itself, but rather are the ouput of the peak detection algorihtm, superimposed on the solution. Likewise, the nerve outlines on the floors of figures c)-f) are not part of the source localization, but have been added to help the reader visualize the location of the pathways within the nerve (idealized anatomy for the estimated pathways in Figures c) and d), and realistic anatomy for the true pathways in Figures e) and f)).

and problems of this class can only be solved satisfactorily if sufficient appropriate constraints are imposed on the solution. We therefore compared the performance of the approach using idealized and correct models of the nerve geometry, and in the presence of a spatio-temporal constraint based on the electrophysiology of myelinated nerve fibres. As expected, the overall performance improved as more information was incorporated. Nonetheless, most of the simulated cases had mean localization errors in the 150μm to 180μm range (in a 720μm-diameter endoneurium, with 10μm-diameter individual fibres), and unacceptably high numbers of spurious pathways. Only at very low noise levels and with accurate constraints did the performance reach levels that would make the approach reliably usable in practice. Even in those situations, however, the number of missed pathways was high, due partly to the low resolution of the sLORETA method. Note that the decrease in the number of missed pathways as noise increased in the

three-pathways case is related to the way that the metrics were computed. Recall that each true pathway is associated with the closest estimated pathway. Therefore, if there are several spurious estimated pathways distributed across the region, then there is a greater chance that some of them will be associated with a true pathway and therefore reduce the number of missed pathways. This explains why the number of missed pathways decreases as the number of spurious pathways increases, and furthermore why cases that have the best performance in the other metrics (e.g. the combination of the correct leadfield and the spatio-temporal constraint) have more missed pathways. In light of this limitation of our metrics, the most revealing values for the number of missed pathways are the ones corresponding to cases with very few spurious pathways. For instance, the simulations using the correct leadfield with the constraint at 0% and 10% noise have close to 0 spurious pathways. In those cases, the number of missed pathways is approximately
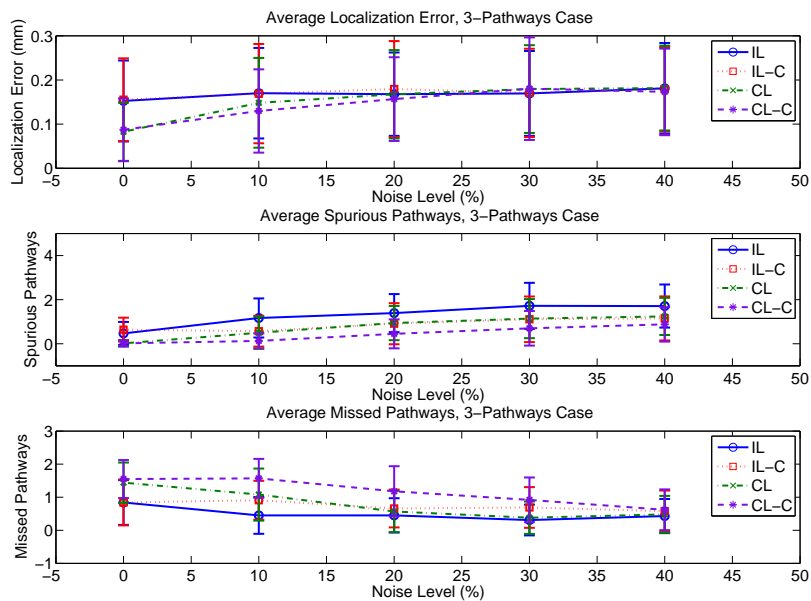
Fig. 4. Localization errors, spurious pathways, and missed pathways for the three-pathways case (n = 100). IL: idealized leadfield; IL-C: idealized leadfield with spatio-temporal constraint; CL: correct leadfield; CL-C: correct leadfield with spatio-temporal constraint.

1.5, or half the number of true pathways. This is a very high proportion, but it is not entirely unexpected. Recall that sLORETA imposes smoothness on the solution, and therefore is not capable of reliably distinguishing closely spaced sources. Therefore, if two pathways are close to one another, they will be lumped together in the estimate, thereby producing missed pathways. In addition, our determination of the location of the estimated pathways is based on local maxima. Upon visual inspection, however, it becomes clear that pathways do not always produce local maxima, but may significantly affect the shape of the solution in other ways (for example by producing elongated ridges). There is therefore a need for a better method of identifying the estimated pathways, but given the variability of shapes and magnitudes that may occur this is not a trivial problem and is outside the scope of this paper.

Some remarks are in order regarding the way that information was incorporated into the problem in this study. The simulations that use the correct leadfield and no noise should be considered a mostly theoretical situation useful for examining the effects of adding information, because such an exact correspondence will never be found in practice, even if detailed anatomical information is available. On the other hand, when noise is incorporated into the simulations, it can be interpreted as a combination of measurement noise and geometry noise (i.e. mismatch between the leadfield and reality), such that the simulations with high noise may be more indicative of the expected performance in practical situations where anatomical information is available. As for the spatio-temporal constraint, it has already been mentioned that, in the absence of anatomical information about the layout of fibre types in the nerve, it is useful only if a single type of fibre dominates the nerve's activity at a given time. Although it is feasible to ascertain in practice whether or not this assumption

is reasonable [43], it does nonetheless restrict the range of practical situations in which the constraint would be usable. It is therefore also used in this paper as much as a theoretical tool to examine the effects of constraints as a suggestion for a practical technique. Overall, there is no doubt that more work is required to develop constraints that are both useful from the point of view of the inverse problem and whose practical implementation is realistic.

More generally, if the peripheral nerve source localization approach is ever to be usable as part of a neuroprosthetic system, several advancements are needed. First, noise reduction is essential, and could take the form of improved instrumentation, better isolation of external signals at the cuff level, or neuro-modulation techniques to boost the amplitude of the recorded nerve signal [46]. Second, methods should be investigated to obtain precise images of a nerve's anatomy *in vivo*. For example, an adaptation of electrical impedance tomography techniques [47] to peripheral nerves could be considered, and studies have already shown that fascicles within a nerve can be imaged using ultrasound [48]. It is interesting to note, however, that in our simulations the performance using only the spatio-temporal constraint with the idealized leadfield (IL-C) was not very far from that using only the correct leadfield without the spatio-temporal constraint (CL), at least for cases with non-zero noise. This raises the possibility that if sufficient physiological and contextual information could be provided as constraints, and the noise brought down to a manageable level, then an idealized geometry could perhaps still be used. This would be analogous to using a three-sphere head model in the EEG/MEG source localization problem, as opposed to a patient-specific MRI-based anatomical model. Another cause for cautious optimism is that the performance for the very idealized case of noiseless measurements and full constraints

approached acceptable levels, which implies that the very large number of dipoles in the region (50 per pathway in this study) may not be an insurmountable obstacle in itself to pathway localization. Importantly, although this study was written with an eye to applying the method to neuroprosthetic systems, the potential for neural system identification (in this case identifying the peripheral control signals involved in specific tasks) is also very interesting, and has a different set of restrictions. In particular, in a context where repeated trials and off-line processing options are available, the noise could be significantly reduced by trial averaging and a wider range of algorithms explored, since computation time would no longer be as much of an issue. It may therefore be worthwhile to keep exploring the source localization approach in this context. For neuroprosthetic applications, sub-fascicular resolutions do not appear realistic on the short term, and the usefulness of the method as a framework for determining the activation of combinations of several fascicles will be contingent on future developments like the ones discussed above (particularly if numerous small fascicles are involved, as is more likely to be the case in humans).

The present study aimed to estimate the overall viability of the source localization approach. There are various topics that were not discussed in detail here but would become very relevant if the performance was improved enough to make the approach usable. First, it is important to keep in mind the very high temporal resolution of the method, which is not reflected in the metrics used in this study. For each dipole location, the algorithm produces a complete activation time series, making it possible to study transmembrane current waveforms and firing frequencies for precise locations in the nerve. Second, the influence of the number of contacts on the performance would need to be explored. We limited ourselves here to using a model of an existing electrode, but as manufacturing techniques improve so will the number of contacts that can be placed on a cuff, and this will undoubtedly have an influence on the source localization performance. There may also be a plateau to the benefits of increasing the number of contacts, such that the optimal number should be sought. Third, the number of pathways that the method can accurately localize in a given situation should be determined. The use of three pathways in this study was motivated by the need to study a simple multi-pathway case, rather than by physiological considerations. That said, the term "pathway" should not necessarily be equated with a single nerve fibre, particularly given the limited resolution and the coarseness of the mesh. Multiple closely spaced nerve fibres that have a functional relationship and a roughly synchronous firing pattern (e.g. compound action potential) may therefore be considered a single pathway, as could a very small fascicle. Similarly, the currents generated by a few isolated nerve fibres that fire at the same time as a larger coordinated group of fibres elsewhere in the nerve may be drowned out and confused with noise; in that case, they may be missed by the algorithm, but may not significantly hamper the localization of the "main" pathway. The last issue that deserves to be discussed is that of computation time. Our choice of algorithm was partially based on its speed. On a 2.33GHz dual-processor

workstation, localization for a single time instant using the idealized leadfield and no constraints took approximately 1 second. When using the correct leadfield or the spatio-temporal coupling, the computation time increased roughly proportionally to the number of variables to be solved for. While these computation times are not yet suitable for real-time implementation, it is nonetheless a realistic target as computational speed continues to increase and more efficient implementations of the algorithm are explored. As mentioned earlier, in situations where speed is not an issue, slower algorithms could be explored, for example ones based on Lp norms (e.g. [25]).

REFERENCES

[1] S. H. Scott, "Optimal feedback control and the neural basis of volitional motor control," *Nat. Rev. Neurosci.*, vol. 5, no. 7, pp. 532–546, Jul 2004.

[2] N. J. Rijkhoff, "Neuroprostheses to treat neurogenic bladder dysfunction: current status and future perspectives," *Childs Nerv. Syst.*, vol. 20, no. 2, pp. 75–86, Feb 2004.

[3] M. Sahin and D. M. Durand, "Selective recording with a multi-contact nerve cuff electrode," in *Proc. 18th Ann. Int. Conf. of the IEEE Eng. in Med. and Biol. Soc.*, Amsterdam, Netherlands, 1996, pp. 369–370.

[4] J. Perez-Orive and D. M. Durand, "Modeling study of peripheral nerve recording selectivity," *IEEE Trans. Rehab. Eng.*, vol. 8, no. 3, pp. 320–329, Sep 2000.

[5] M. Sahin, "Noise tolerance as a measure of channel discrimination for multi-channel neural interfaces," in *Proc. 23rd Ann. EMBS Int. Conf.*, Istanbul, Turkey, 2001, pp. 704–706.

[6] P. B. Yoo and D. M. Durand, "Selective recording of the canine hypoglossal nerve using a multicontact flat interface nerve electrode," *IEEE Trans. Biomed. Eng.*, vol. 52, no. 8, pp. 1461–1469, Aug 2005.

[7] X. Navarro, T. B. Krueger, N. Lago, S. Micera, T. Stieglitz, and P. Dario, "A critical review of interfaces with the peripheral nervous system for the control of neuroprostheses and hybrid bionic systems," *J. Peripher. Nerv. Syst.*, vol. 10, no. 3, pp. 229–258, Sep 2005.

[8] M. S. Hamalainen and R. J. Ilmoniemi, "Interpreting magnetic fields of the brain: minimum norm estimates," *Med. Biol. Eng. Comput.*, vol. 32, no. 1, pp. 35–42, Jan 1994.

[9] R. D. Pascual-Marqui, C. M. Michel, and D. Lehmann, "Low resolution electromagnetic tomography: a new method for localizing electrical activity in the brain," *Int. J. Psychophysiol.*, vol. 18, no. 1, pp. 49–65, Oct 1994.

[10] R. D. Pascual-Marqui, "Standardized low-resolution brain electromagnetic tomography (sLORETA): technical details," *Methods Find. Exp. Clin. Pharmacol.*, vol. 24 Suppl D, pp. 5–12, 2002.

[11] C. Phillips, M. D. Rugg, and K. J. Friston, "Anatomically informed basis functions for EEG source localization: combining functional and anatomical constraints," *NeuroImage*, vol. 16, no. 3 Pt 1, pp. 678–695, Jul 2002.

[12] R. Grave de Peralta Menendez, M. M. Murray, C. M. Michel, R. Martuzzi, and S. L. G. Andino, "Electrical neuroimaging based on biophysical constraints," *NeuroImage*, vol. 21, no. 2, pp. 527–539, Feb 2004.

[13] C. Phillips, J. Mattout, M. D. Rugg, P. Maquet, and K. J. Friston, "An empirical Bayesian solution to the source reconstruction problem in EEG," *NeuroImage*, vol. 24, no. 4, pp. 997–1011, Feb 15 2005.

[14] M. K. Haugland and T. Sinkjaer, "Cutaneous whole nerve recordings used for correction of footdrop in hemiplegic man," *IEEE Trans. Rehab. Eng.*, vol. 3, no. 4, pp. 307–317, 1995.

[15] B. Upshaw and T. Sinkjaer, "Digital signal processing algorithms for the detection of afferent nerve activity recorded from cuff electrodes," *IEEE Trans. Rehab. Eng.*, vol. 6, no. 2, pp. 172–181, Jun 1998.

[16] S. Jezernik and W. M. Grill, "Optimal filtering of whole nerve signals," *J. Neurosci. Meth.*, vol. 106, no. 1, pp. 101–110, Mar 30 2001.

[17] G. A. Kurstjens, A. Borau, A. Rodriguez, N. J. Rijkhoff, and T. Sinkjaer, "Intraoperative recording of electroneurographic signals from cuff electrodes on extradural sacral roots in spinal cord injured patients," *J. Urol.*, vol. 174, no. 4 Pt 1, pp. 1482–1487, Oct 2005.

[18] W. Tesfayesus and D. M. Durand, "Blind source separation of peripheral nerve recordings," *J. Neural Eng.*, vol. 4, no. 3, pp. S157–67, Sep 2007.

[19] B. K. Lichtenberg and C. J. D. Luca, "Distinguishability of functionally distinct evoked neuroelectric signals on the surface of a nerve," *IEEE Trans. Biomed. Eng.*, vol. 26, no. 4, pp. 228–237, Apr 1979.

[20] H. S. Cheng, M. S. Ju, and C. C. Lin, "Estimation of peroneal and tibial afferent activity from a multichannel cuff placed on the sciatic nerve," *Muscle Nerve*, vol. 32, no. 5, pp. 589–599, Nov 2005.

[21] M. A. Moffitt and W. M. Grill, "Electrical localization of neural activity in the dorsal horn of the spinal cord: a modeling study," *Ann. Biomed. Eng.*, vol. 32, no. 12, pp. 1694–1709, Dec 2004.

[22] C. M. Michel, M. M. Murray, G. Lantz, S. Gonzalez, L. Spinelli, and R. G. de Peralta, "EEG source imaging," *Clin. Neurophysiol.*, vol. 115, no. 10, pp. 2195–2222, Oct 2004.

[23] J. C. Mosher, R. M. Leahy, and P. S. Lewis, "EEG and MEG: forward solutions for inverse methods," *IEEE Trans. Biomed. Eng.*, vol. 46, no. 3, pp. 245–259, Mar 1999.

[24] D. Sharon, M. S. Hamalainen, R. B. Tootell, E. Halgren, and J. W. Belliveau, "The advantage of combining MEG and EEG: Comparison to fMRI in focally stimulated visual cortex," *NeuroImage*, vol. 36, no. 4, pp. 1225–1235, Jul 15 2007.

[25] P. Xu, Y. Tian, H. Chen, and D. Yao, "Lp norm iterative sparse solution for EEG source localization," *IEEE Trans. Biomed. Eng.*, vol. 54, no. 3, pp. 400–409, 2007.

[26] D. Weinstein, L. Zhukov, and C. Johnson, "Lead-field bases for electroencephalography source imaging," *Ann. Biomed. Eng.*, vol. 28, no. 9, pp. 1059–1065, 2000.

[27] M. Seger, G. Fischer, R. Modre, B. Messnarz, F. Hanser, and B. Tilg, "Lead field computation for the electrocardiographic inverse problem–finite elements versus boundary elements," *Comput. Methods Programs Biomed.*, vol. 77, no. 3, pp. 241–252, Mar 2005.

[28] M. Schuettler, I. F. Triantis, B. Rubehn, and T. Stieglitz, "Matrix cuff electrodes for fibre and fascicle selective peripheral nerve recording and stimulation," in *Proc. 12th Ann. Conf. IFESS*, Philadelphia, PA, 2007.

[29] H. Schmalbruch, "Fiber composition of the rat sciatic nerve," *Anat. Rec.*, vol. 215, no. 1, pp. 71–81, May 1986.

[30] E. V. Goodall, L. M. Kosterman, J. Holsheimer, and J. J. Struijk, "Modeling study of activation and propagation delays during stimulation of peripheral nerve fibers with a tripolar cuff electrode," *IEEE Trans. Rehab. Eng.*, vol. 3, pp. 272–282, 1995.

[31] S. Parrini, J. Delbeke, E. Romero, V. Legat, and C. Veraart, "Hybrid finite elements and spectral method for computation of the electric potential generated by a nerve cuff electrode," *Med. Biol. Eng. Comput.*, vol. 37, no. 6, pp. 733–736, Nov 1999.

[32] J. H. Meier, W. L. C. Rutten, and H. B. K. Boom, "Extracellular potentials from active myelinated fibers inside insulated and noninsulated peripheral nerve," *IEEE Trans. Biomed. Eng.*, vol. 45, no. 9, pp. 1146–1154, 1998.

[33] A. Q. Choi, J. K. Cavanaugh, and D. M. Durand, "Selectivity of multiple-contact nerve cuff electrodes: a simulation analysis," *IEEE Trans. Biomed. Eng.*, vol. 48, no. 2, pp. 165–172, Feb 2001.

[34] E. Romero, J. F. Denef, J. Delbeke, A. Robert, and C. Veraart, "Neural morphological effects of long-term implantation of the self-sizing spiral cuff nerve electrode," *Med. Biol. Eng. Comput.*, vol. 39, no. 1, pp. 90–100, Jan 2001.

[35] SCIRun: A Scientific Computing Problem Solving Environment. Scientific Computing and Imaging Institute (SCI), http://software.sci.utah.edu/scirun.html, 2002.

[36] J. D. Sweeney, J. T. Mortimer, and D. Durand, "Modeling of mammalian myelinated nerve for functional neuromuscular stimulation," in *Proc. 9th Ann. Int. Conf. IEEE Eng. Med. Biol. Soc.*, 1987, pp. 1577–1578.

[37] R. Plonsey, "Action potential sources and their volume conductor fields," *Proc. IEEE*, vol. 65, no. 5, pp. 601–611, 1977.

[38] J. C. Mosher, P. S. Lewis, and R. M. Leahy, "Multiple dipole modeling and localization from spatio-temporal meg data," *IEEE Trans. Biomed. Eng.*, vol. 39, no. 6, pp. 541–557, Jun 1992.

[39] J. C. Mosher and R. M. Leahy, "Recursive MUSIC: a framework for EEG and MEG source localization," *IEEE Trans. Biomed. Eng.*, vol. 45, no. 11, pp. 1342–1354, Nov 1998.

[40] J. Malmivuo and R. Plonsey, *Bioelectromagnetism : principles and applications of bioelectric and biomagnetic fields*. New York: Oxford University Press, 1995.

[41] R. D. Pascual-Marqui, "Review of methods for solving the EEG inverse problem," *IJBEM*, vol. 1, no. 1, pp. 75–86, 1999.

[42] ——, "Reply to comments made by R. Grave de Peralta Menendez and S.L. Gozalez Andino," *IJBEM*, vol. 1, no. 2, 1999.

[43] R. Rieger, J. Taylor, E. Comi, N. Donaldson, M. Russold, C. M. Mahony, J. A. McLaughlin, E. McAdams, A. Demosthenous, and J. C. Jarvis, "Experimental determination of compound action potential direction and propagation velocity from multi-electrode nerve cuffs," *Med. Eng. Phys.*, vol. 26, no. 6, pp. 531–534, Jul 2004.

[44] F. Darvas, U. Schmitt, A. K. Louis, M. Fuchs, G. Knoll, and H. Buchner, "Spatio-temporal current density reconstruction (stCDR) from EEG/MEG-data," *Brain Topogr.*, vol. 13, no. 3, pp. 195–207, Spring 2001.

[45] U. Schmitt, A. K. Louis, F. Darvas, H. Buchner, and M. Fuchs, "Numerical aspects of spatio-temporal current density reconstruction from EEG-/MEG-data," *IEEE Trans. Med. Imaging*, vol. 20, no. 4, pp. 314–324, Apr 2001.

[46] M. Sahin, D. M. Durand, and M. A. Haxhiu, "Improved nerve cuff electrode recordings by sub-threshold anodic currents," in *Proc. 17th Ann. Conf. IEEE Eng. in Med. and Biol. Soc.*, Montreal, Canada, 1995, pp. 1107–1108.

[47] B. H. Brown, "Electrical impedance tomography (EIT): a review," *J. Med. Eng. Technol.*, vol. 27, no. 3, pp. 97–108, May-Jun 2003.

[48] H. Kubiena, M. Hormann, W. Michlits, M. Tschabitscher, K. Groszschmidt, and M. Frey, "Intraoperative imaging of the brachial plexus by high-resolution ultrasound," *J. Reconstr. Microsurg.*, vol. 21, no. 7, pp. 429–433, Oct 2005.

José Zariffa received the M.A.Sc. degree from the departments of electrical and biomedical engineering at the University of Toronto, Canada, in 2004, and the B.Eng. degree in computer engineering from McGill University in 2002. He is currently pursuing Ph.D. studies in electrical and biomedical engineering at the University of Toronto. His research interests are in neural interfaces, neuroprostheses, neural modeling, and bioelectric source localization.

Milos R. Popovic received the Ph.D. degree in mechanical engineering from the University of Toronto, Canada in 1996, and the Dipl. Electrical Engineer degree from the University of Belgrade, Yugoslavia in 1990.

Dr. Popovic is Toronto Rehab Chair in Spinal Cord Injury Research. He is also an Associate Professor in the Institute of Biomaterials and Biomedical Engineering at the University of Toronto, and Senior Scientist and the Activity Team Leader at Toronto Rehabilitation Institute, both institutions located in Toronto, Canada.

Dr. Popovic joined the Institute of Biomaterials and Biomedical Engineering and the Toronto Rehab in 2001. From 1997 until 2001 he was leading the Rehabilitation Engineering Team at the Swiss Federal Institute of Technology (ETH) and the Paraplegic Center of the University Hospital Balgrist, both in Zurich, Switzerland. From 1996 until 1997, he worked for AlliedSignal Aerospace Canada Inc. in Toronto, Canada.

Dr. Popovic's fields of expertise are functional electrical stimulation, neuro-rehabilitation, modeling and control of linear and non-linear dynamic systems, robotics, power systems, signal processing, and safety analysis. His interests are in the areas of neuro-rehabilitation, physiological control systems, assistive technology, and brain machine interfaces. In 1997, together with Dr. Thierry Keller he received the Swiss National Science Foundation Technology Transfer Award - 1st place. In 2008, Dr. Popovic received Research and Development Award from the Professional Engineers of Ontario and Ontario Society of Professional Engineers. He is also one of the co-founders of the Canadian National Spinal Cord Injury Conference established in 2004.